Improved design for SOI based evanescently coupled multilayer spot-size converter

Niharika Kohli, [1] ✉

Email niharika_kohli@yahoo.co.in

B. M. A. Rahman, [2]

Enakshi K. Sharma, [1]

[1] Department of Electronic Science, University of Delhi South Campus, Benito Juarez Road, New Delhi, 110021 India

[2] School of Mathematics, Computer Science and Engineering, City, University of London, Northampton Square, London, EC1V 0HB UK

Abstract

We report an improved version of a spot-size converter (SSC) consisting of a silicon nanowire evanescently coupled to a phase-matched Poly-Si multilayer structure. With wider transversal dimensions the multilayer structure expands the mode significantly thus increasing the coupling efficiency with the conventional single-mode fiber. Detailed optimization process of a 17-layer based SSC is discussed and its coupling efficiency with a high-NA fiber of radius 2 μm is obtained as 98% providing only 0.087 dB loss. Vertical alignment tolerance between the optimized SSC and a high-NA fiber of radius 2 μm is also shown. This novel design does not consist of a taper and can be fabricated by using CMOS compatible process. It has a short device length and more relaxed alignment tolerances with the fiber. Full-vectorial and computationally efficient finite element method and the least squares boundary residual method have been used for the analysis and optimization of the proposed structure.

Keywords

1. Introduction

Silicon photonics has opened doors to many applications with numerous benefits. The use of silicon as the material for photonic devices has led to miniaturization of the waveguides and reduced the overall production costs. This is due to the fact that the chips can now be mass produced with the fabrication steps being compatible with the well-established CMOS technology used by the semiconductor industries. One of the major obstacles that still remains in implementing its wider application is to reduce loss when coupling the nanowire waveguide to an input or output fiber. The mode-size area of the nanowire typically used is ~0.1 μm^2 whereas this area of a typical single-mode fiber of radius 5 μm is ~80 μm^2. Due to a large mode mismatch the direct butt-coupling between the fiber and the nanowire leads to a huge power loss (Tsuchizawa et al. 2005). Therefore development of an efficient coupling technology is very important for the proper functioning of the silicon based optical system.

Microlenses or lensed fibers can be used for this purpose. However, because of the small size of the microlens they are difficult to align and also require very stringent alignment tolerances. Similarly, the lensed fibers require alignment machinery for accurate positioning of the fiber with the waveguide. This escalates the cost of the overall chip production and hinders global ambition of the fiber-to-the-home, 'FTTH'. Therefore, researchers have considered some new types of spot-size converters such as tapered waveguide structures (Tsuchizawa et al. 2005; Haxha et al. 2006; Bakir et al. 2010; Fang et al. 2010; Tokushima et al. 2012), and grating couplers (Taillaert et al. 2002, 2006), to overcome the stringent alignment issues.

Tapered waveguide devices can have vertical, horizontal or simultaneously both vertical and horizontal tapering. The spot-size of the nanowire mode can slowly be reduced along the taper till the core reaches its cut-off and the mode is expanded and transferred to a secondary core built around this primary core. Although the idea of tapered waveguides is very interesting, it suffers from some major drawbacks. For example, the width of the tapered waveguide at the end cannot be practically reduced to zero. Therefore, the structure suffers from undesirable reflection from this abrupt termination. Such feedback can deteriorate performance

in case of active devices, such as, lasers or amplifiers. Besides that the secondary core might often be multimoded. Another disadvantage is the complicated fabrication steps required to produce a vertical taper. Some of these recent tapered SSC's include those providing <1 dB loss (Bakir et al. 2010), suspended waveguides (Fang et al. 2010) and dual tapered double core structures (Tokushima et al. 2012).

Grating coupler fabricated horizontally on the chip to transfer power from the waveguide to the optical fiber also presents itself as a promising candidate. However, it is highly polarization dependent and light is generally coupled out of plane from fiber to the waveguide (Cheng and Tsang 2014). As a grating coupler is also strongly wavelength dependent, so they have very narrow operating bandwidths (Cheng et al. 2012a, b).

A spot-size converter (SSC) based on a different design concept (Jiang et al. 2016) has been recently reported. This SSC comprises of two evanescently coupled waveguides: a standard nanowire and a phase-matched array of Polycrystalline-Silicon waveguides. The array is designed to have a much larger width than the nanowire, thus expanding the mode horizontally in the x direction. Similarly due to a number of cores arranged vertically the mode expands in the vertical y direction as well. A recently published SSC exploits a similar structure for mode expansion using Si_3N_4 layers in the upper cladding to increase the effective refractive index of the cladding (Papes et al. 2016). The schematic depicting the coupling between the nanowire and a fiber using the SSC of length L presented in this paper is shown in Fig. 1a where the arrows depict the direction of light propagation. The cross-section of this SSC is shown in Fig. 1b. Since the structure is symmetric in the x direction, only half of the structure was simulated by enforcing a symmetric wall along the vertical y-axis. Here, W_1 and H represent the width and height of the nanowire (NW), respectively. The width of the array is shown as W_2. Here, s is the separation between the array and the NW, h and s_p are the height of the multi-Poly-Si layers and the inner separation between them in the array section, respectively. The dimensions for the NW are $W_1 \times H = 400 \times 220$ nm and the width W_2 for the array is 6 μm. The refractive indices for Si, Poly-Si and SiO_2 are taken as 3.47548, 3.48 and 1.46 (Preston et al. 2007; Barh et al. 2013) respectively, at the operating wavelength of 1.55 μm.

Fig. 1

a Schematic diagram for coupling between NW, multilayer based SSC and fiber, **b** cross-section of spot-size converter structure consisting of coupled Si nanowire and

multilayer Poly-Si structure (Jiang et al. 2016)
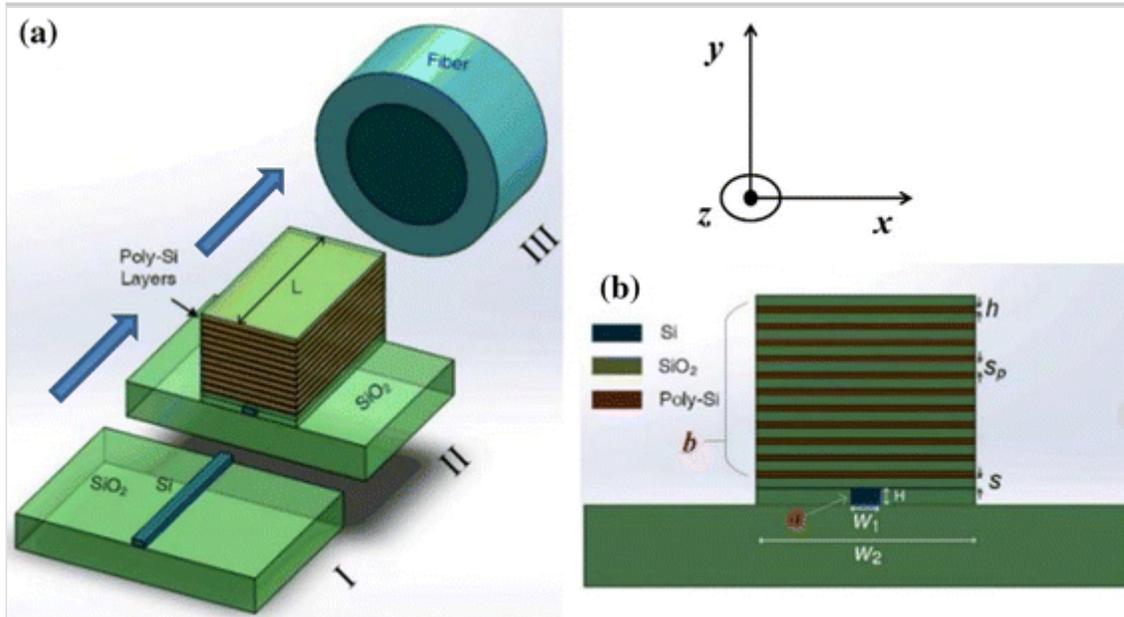
The CMOS compatible fabrication for this SSC would require the plasma enhanced chemical vapor deposition (PECVD) of silica. Poly-Si layers can be deposited as thin films of amorphous silicon by LPCVD and then crystallized by annealing at 600 °C and again at 1100 °C as shown by Preston et al. (2007). The waveguide widths are further defined by etching. An additional mask would be required for the fabrication of multilayer structure after the nanowire formation.

In Jiang et al. (2016) this SSC has been analyzed numerically using the first two supermodes of the composite structure, where the first supermode is the symmetric mode of the NW and array fundamental mode, and the second supermode is the antisymmetric mode. The height h of the Poly-Si layers in the array can be tuned to obtain the point of minimum separation between these two supermodes. At this phase-matching, both the supermodes have equal power in the NW and the array. If we input power in the NW, using this optimized height h we observe power transfer from the NW to the array such that at the end of SSC section (corresponding to the coupling length) the field is identical to the fundamental mode of the array. At the end of the SSC, a single-mode fiber (SMF) can be placed in alignment with the SSC for a high coupling efficiency between the NW and the SMF.

In this paper we present an enhanced version of this SSC. Since the array is multimoded, we have now taken also into consideration the existence of possible higher order modes of the composite structure. The assumption taken into account in Jiang et al. (2016) that only two modes of the SSC can be used in the analysis

may not be valid in some cases. In this paper we present these design criteria in detail based on which a new optimized design with improved coupling efficiency with the fiber is proposed.

We also report the coupling between the optimized multilayer array of the SSC with SMF of varying radii to find the fiber size which will provide maximum coupling. Finally, we find the coupling efficiency between the optimized SSC and this high-NA fiber. We have also studied the vertical alignment tolerance between this fiber and the SSC. We have used an in-house numerically efficient full-vectorial algorithm for finite element method (FEM) to analyse the modal characteristics of the spot-size converter (Rahman and Davies 1984), and the least squares boundary residual (LSBR) method to analyse power coupling at the junctions (Rahman and Davies 1988). Both the FEM and LSBR method used here represent a powerful and efficient tool to analyse structure such as ours (Wongcharoen et al. 2001; Rajarajan et al. 1996; Wongcharoen et al. 1996). The LSBR method is used to calculate the power transfer efficiency by imposing the continuity of the field at the junction interface in a least squares sense and obtain the modal coefficients of the transmitted and reflected fully hybrid modes at the discontinuity interface.

2. Design analysis

### 2.1. Previous design

In the previous design of Jiang et al. (2016), an 11-layer based SSC with $h = 105$ nm, $s_p = 400$ nm, and s = 200 nm was studied. Although the Poly-Si layers were single-moded vertically but it should be noted that they can support higher order modes laterally. Similarly the multilayer coupled structure also supports many supermodes vertically. A particular case was considered, which excited many higher order modes at the NW and SSC-array junction. The excitation coefficient of the jth mode from the ith input mode at a junction in the system is defined as $C_{ij} = \int (E_{xi} H_{yj} - E_{yi} H_{xj}) \cdot dx \cdot dy$. It was observed that the excitation coefficients for some of the higher-order supermodes of this SSC were comparable to the excitation coefficients of the first two supermodes of the SSC. Figure 2 shows the bar graph for the excitation coefficients of the first 30 modes of this SSC along with an inset showing the first and second supermode fields. The highest values of excitation coefficients correspond to the symmetric modes in the horizontal x direction. For example, mode 1, 2, 4 and 6 are first symmetric mode in x, mode 10, 14, 17 and 19 are second symmetric in x and 21, 23 and 29 are third symmetric in x.

This is expected because the input mode in the NW is first symmetric in x and therefore will excite only the symmetric modes of the SSC.

Fig. 2

Excitation coefficients for the first 30 supermodes of a SSC design with 11-layers having $h = 105$ nm, $s_p = 400$ nm and s = 200 nm along with an *inset* showing the first and second supermode fields
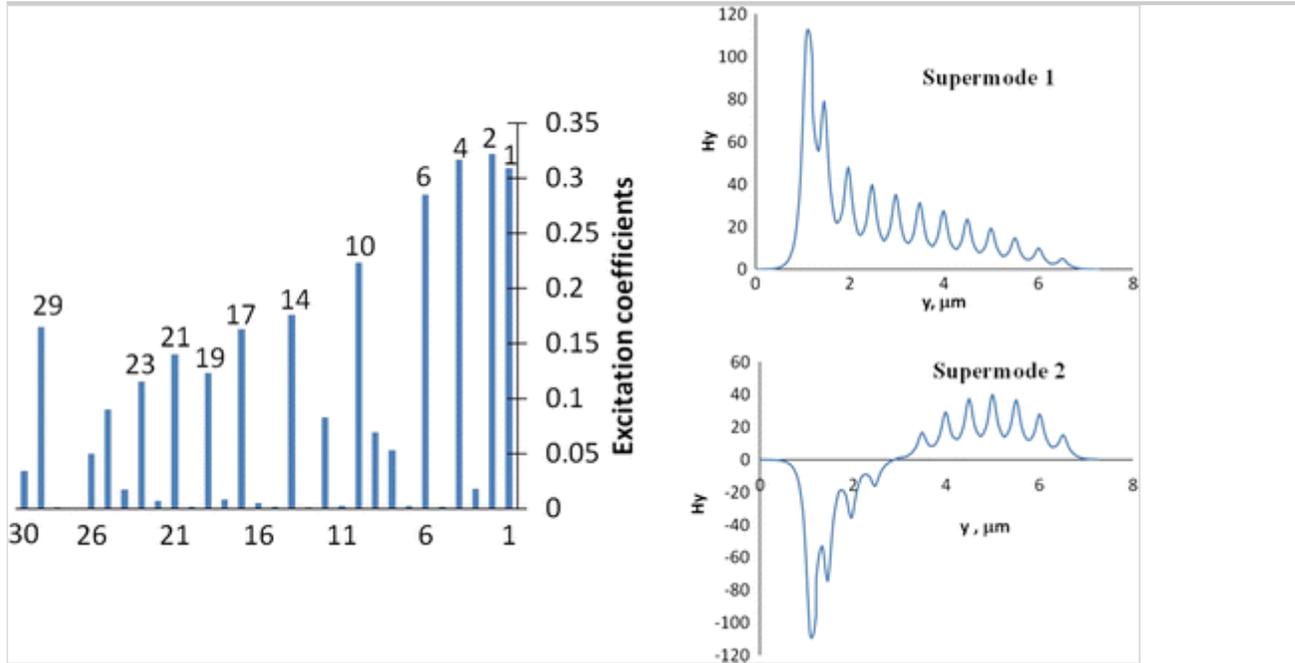
During the design analysis for our SSC, we found that the first two supermodes have much higher excitation coefficients than the higher order modes only particularly in the case where the NW and array behave as two distinct waveguides in the composite structure. This can be achieved mostly when the spacing between NW and array is greater than the inner separation between the Poly-Si layers of the array. If the spacing between the NW and the next single Poly-Si waveguide is smaller than the inner separation of the array, the NW and the single Poly-Si layer become one distinct waveguide and the rest of the array behaves as the other distinct section.

We next simulate the 11 layers based SSC having $s_p = 400$ nm with a separation $s > s_p$. We now consider a larger separation s = 500 nm. On changing the separation between the NW and the array, the phase-matching point between the supermodes will shift. Now, the point of minimum separation between the supermodes is at $h = 95$ nm. When we input power from the NW into the SSC, we obtain the first two supermode excitation coefficients as 0.58 and 0.77. The coupling length

corresponding to the first two supermodes is 493 μm where the field shape resembles the fundamental array mode. Since the first two supermodes carry most of the power in this design, even after including 30 modes in the numerical analysis the field at the coupling length is unaltered. This analysis has been carried out using the finite element method (FEM) and eigen mode expansion method of the photon design tool.

In order to have a shorter coupling length, a smaller value of separation s between array and NW is required. To satisfy the above mentioned design-rule we have to keep the inner separation of array, s_p, smaller than s. To compensate for the reduced overall vertical dimension, the number of layers in the SSC can be increased. Therefore, in the following section we carry out a detailed design analysis and optimization for a 17-layer based SSC.

2.2. Optimization strategy

The important design parameters studied in this paper include the effective index (n_e), spot-size and effective area (A_{eff}) of the modes of the SSC. Here, FEM has been used to find the n_e and the field profile of the concerned structure. The spot-size of the mode can be defined as the area, σ, where power density is higher than s^{max}/e^2 when s^{max} is the highest power density. The effective area, A_{eff}, can be calculated from the following expression (Uthman et al. 2012):

$$\mathbf{A}_{eff} = \frac{\left(\iint |E_t|^2 \, dxdy\right)^2}{\iint |E_t|^4 \, dxdy} \qquad 1$$

where E_t is the transverse electric field vector and integration is carried out over the whole cross-section of the waveguide. If the field profile is Gaussian in shape, then both these values are identical. However, in this study as the field profile of the SSC will not be Gaussian, both these parameters are evaluated in this work. We now present a detailed design analysis and optimization strategy for our 17-layer based SSC.

2.2.1. Nanowire

A typical NW may have dimensions, width, $W_1 = 500$ nm and height, $H = 220$ nm. The effective index of this NW is calculated first and its accuracy is tested with the changing mesh size. Variation of the effective index with the mesh size is shown in Fig. 3. In this case same number of mesh divisions are used in both the transverse

directions. It can be observed that as the mesh division is increased the effective index converges to a stable value. Besides that, a powerful Aitken's extrapolation technique (Rahman and Davies 1985), is also used to further enhance the computational accuracy and the resulting effective index value is found to be 2.383 for this NW. The spot-size and A_{eff} of this NW are obtained as 0.101 and 0.108 μm^2, respectively.

Fig. 3

Effective index variation with the mesh size for the silicon nanowire
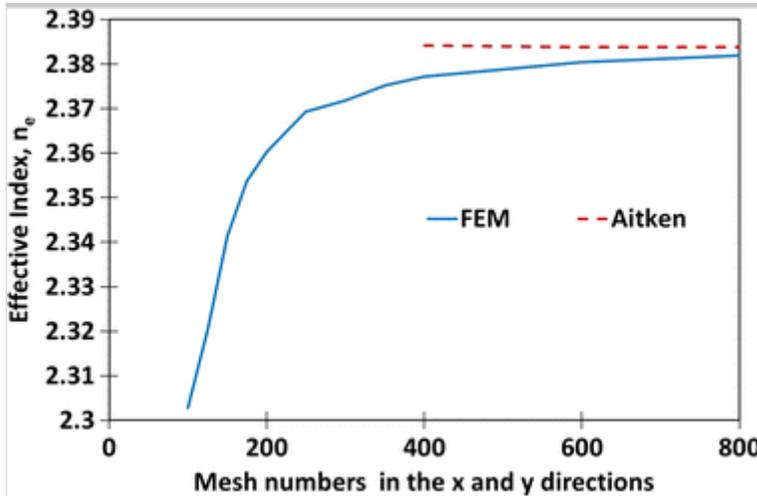

2.2.2. Effect of thickness 'h' on Si multilayer array

Next, a single Silicon layer (SiL) structure with expanded width of $W_2 = 6$ μm is simulated. This structure has an expanded mode in the horizontal direction and its height 'h' can be adjusted so that it can be phase-matched to the NW. It is observed that when, h is 126 nm, the effective index value is equal to that of the NW, so the waveguides are phase-matched. In this case, the spot-size of this wider SiL is 1.15 μm^2 and A_{eff} is 1.21 μm^2 showing a significant increase in these values compared to the NW.

To further expand the mode in the vertical direction more layers are added to this structure. We have simulated the structure with 3, 7 and 17 layers of thin SiL cores. We deliberately chose the number of layers to be an odd number so that the maximum field value could be obtained at the center of the array and the resulting fundamental mode would resemble closer to a Gaussian shape. Figure 4a shows the 2-D mode profile of a 17 core array with $h = 125$ nm and $s_p = 600$ nm. The field profile has a Gaussian shape along the horizontal direction. Its vertical profile is shown in Fig. 4b and can be clearly observed that the supermode profile of this SiL

array has expanded vertically. Although its envelope has a Gaussian-like shape but lower field intensity in between SiLs are clearly visible. As this would influence coupling to a fiber, an important design parameter that has been taken into account is the ratio of the peak of the mode field at the center (a) and the field value at the adjacent minima (b) in the array (see Fig. 4b). The higher is this (b/a) ratio, closer the field profile would become to a truly Gaussian shape in both the transverse directions.

Fig. 4

a 2-D and **b** 1-D H_y field profile for 17-core array with $W_2 = 6$ μm, $h = 125$ nm and $s_p = 600$ nm
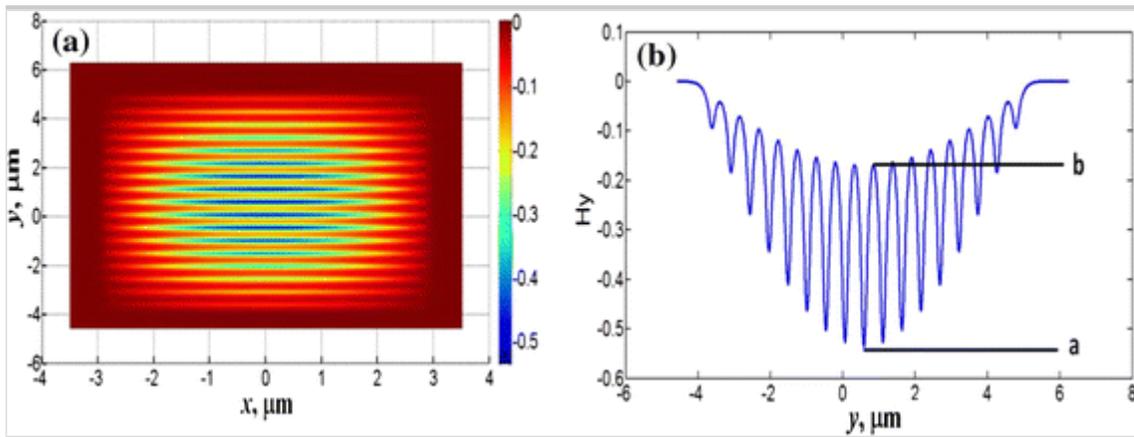
It was observed that by increasing the number of layers (N), the spot-size of the mode can be increased significantly but this multilayer structure must also be phase-matched to the NW. Figure 5 shows the variation of the effective index of this array with the SiL thickness, h, for a single core and 17-cores structure with $s_p = 600$ nm, by a green dash-dotted and a red dashed lines, respectively. It can be observed that the effective index increases linearly with h for both the cases. This value also increases with N but only slightly. To be phase-matched with the NW, h needs to be 126 or 124 nm for a single core or a 17-core array, respectively. Figure 6 shows the A_{eff} of 1-, 3-, 7- and 17-core arrays. The spot-size and A_{eff} for the 17-core array at $h = 124$ nm and $s_p = 600$ nm are 11.23 and 15.21 μm^2, respectively. This is nearly ten times larger than a single SiL and its spot-size and A_{eff} are 101 and 141 times larger than that of the NW spot-size and A_{eff}, respectively. With increasing h value both the spot-size and A_{eff} decrease slightly as the mode becomes more confined in the core and inter-layer coupling reduces (see Fig. 6). Figure 6 also shows ratio (b/a) for the 17-core array. It can be observed that b/a increases with reducing thickness of the core because the mode becomes less confined in the core and spreads more in the adjacent separating regions. It can

be observed from Figs. 5 and 6 that although the effective index is not affected much with the increasing number of layers, but their A_{eff} values drastically increase.

Fig. 5

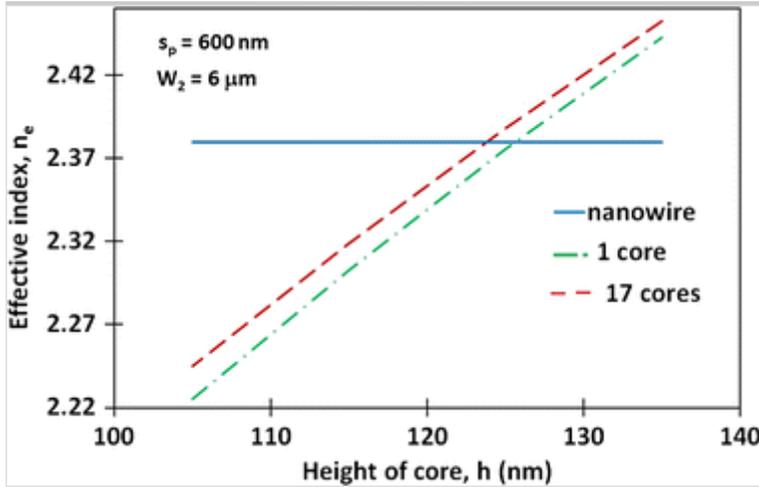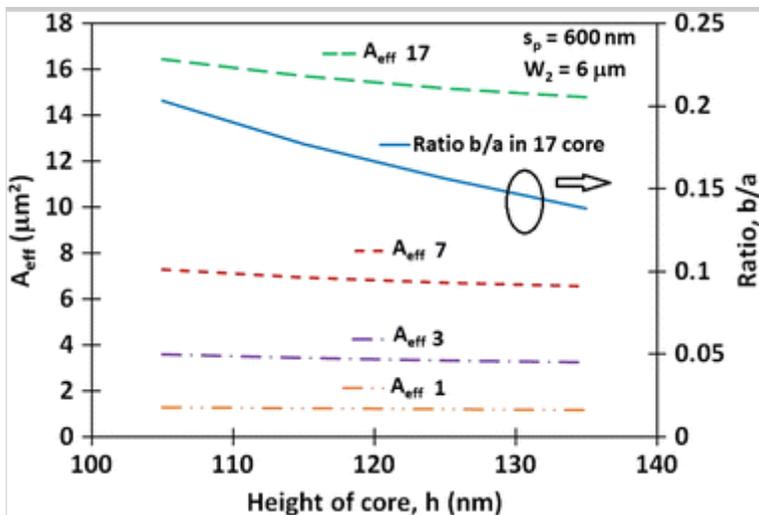Effective index variation for 1- and 17-core array with height of the core, $s_p = 600$ nm and $W_2 = 6$ μm

Fig. 6

A_{eff} and ratio b/a for 1-, 3-, 7- and 17-core array with height of the core, $s_p = 600$ nm and $W_2 = 6$ μm

2.2.3. Effect of spacing 's_p' on Si multilayer array

By increasing the separation (s_p) between the array elements (SiL), its spread can also be increased but this would also reduce b/a ratio by reducing the coupling.

This will also change the effective index of the array but this can also be matched with the NW by simultaneously adjusting the height of the individual SiLs of the array. Figure 7 shows the effect of spacing between the array cores on the effective index for a 2-, 3- and 17-core array for a SiL thickness of $h = 124$ nm. It can be observed that the effective index rises sharply with the reduction of spacing similar to the effective index of an even supermode which increases with the reduced spacing. At a lower spacing (s_p), the thickness of the SiL has to be reduced to keep the array phase-matched to the NW. Although, this will increase the spot-size of the individual layer and the b/a ratio; however reduction of s_p will also reduce the overall height of the array.

Fig. 7

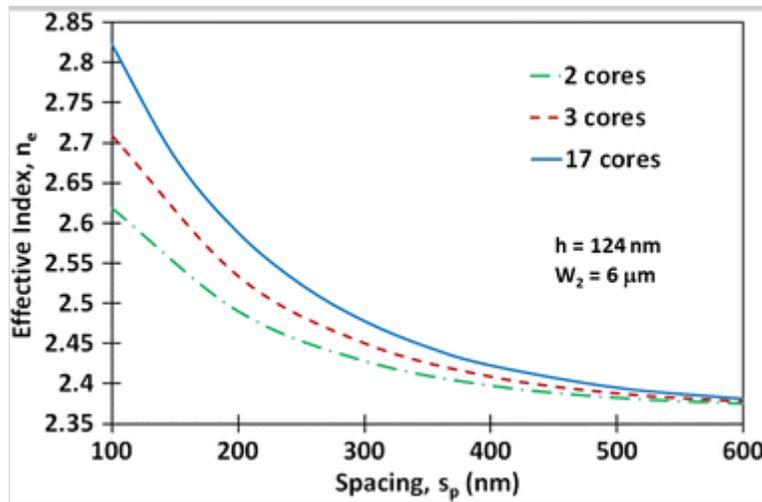Effective index versus array spacing s_p for 2-, 3- and 17-core array

Figure 8 shows the effect of spacing on the spot-size, A_{eff} and ratio b/a for the 17-core array by dashed, solid and dash-dotted lines, respectively. In one set of results, the height of SiL is kept constant at $h = 124$ nm, shown by triangular symbols. However, in the other set along with the spacing, height of SiL is also adjusted to keep the array phase-matched to the NW ($n_e = 2.383$), shown by square symbols. From both the plots it can be observed that the spot-size and A_{eff} first increase with the increase in spacing and then start to drop. It can be observed that as the spacing between the SiL layers, s_p is reduced the b/a ratio increases as the reduced separation increases the coupling strength. It can also be noted that, when h is adjusted to keep phase-matching, resulting b/a ratio is higher compared to that for a fixed h value. As shown in Fig. 7, reduced s_p increases effective index value, so SiL thickness, h, needs to be reduced to maintain the phase-matching, which in turn increases the coupling strength. However, as s_p is increased, the spot-size and A_{eff}

show an initial increase because of the enlargement in the vertical dimension but after reaching a maximum value start to drop because the b/a ratio decreases due to reduced coupling.

Fig. 8

Spot-size, A_{eff} and ratio b/a for 17-core array with fixed h and fixed n_e versus spacing s_p
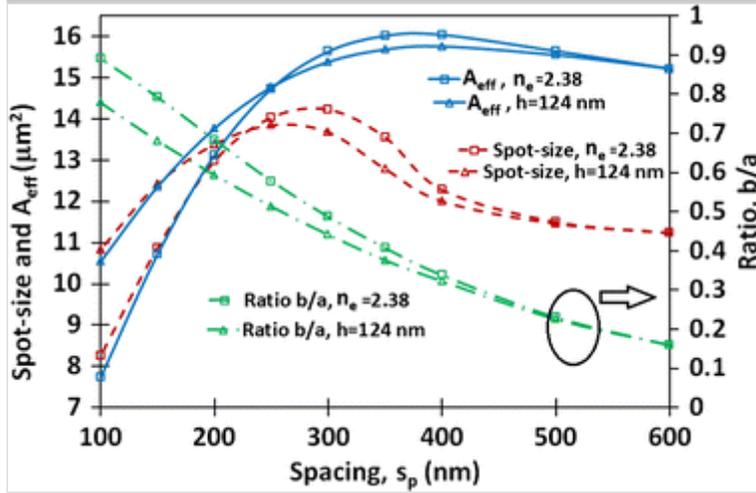
According to Fig. 8, s_p = 400 nm provides the maximum A_{eff} value of 16 μm^2 for the 17-layers based SSC. However, as discussed in Sect. 2.1 in order to have a lower coupling length and satisfy the design criteria of s_p < s, it is best to choose a smaller value of s_p. Moreover, it can be observed from Fig. 8 that at s_p = 200 nm and below, the spot-size and A_{eff} are almost equal and thus the array fundamental field profile is closer to the Gaussian shape profile. Therefore, we choose s_p = 200 nm as the optimized internal separation for the array. The thickness of SiL at this spacing to keep it phase-matched to the NW is h = 89 nm. The spot-size and A_{eff} of the 17-core array in this case were 12.97 and 13.12 μm^2, respectively. Compared to the NW, there is a 127.7 times improvement in the spot-size and 121.3 times improvement in the A_{eff}.

### 2.2.4. Supermodes of the composite structure

Next, the 17-core array coupled with the NW structure is analysed to find its supermodes. We have studied the variation of the first two supermodes of the SSC with the thickness h of the SiL in the array using our algorithm of the finite element method. The point of minimum separation of the supermodes is recorded, and the difference between the supermode effective indices provides the coupling length (L) of the SSC where the power gets transferred from the input NW at z = 0 to the

array fundamental mode. At this stage the effect of s (spacing between the array and the NW) on the supermodes is also analysed.

We first show the supermodes of the 17-layer coupled structure having fixed s_p = 400 nm. As we reduce the value of s from 500 to 400 nm and then to 300 nm, the coupling between the array and NW increases and the gap between the supermodes at the point of minimum separation also increases. This reduces the coupling length of the SSC. Figure 9 shows effective index variation with the SiL thickness, h for the first two supermodes of the structure for three different values of s = 300 nm, 400 and 500 nm.

Fig. 9

First and second supermode effective index versus height of the cores of the 17-core array with s_p = 400 nm for spacing s = 300, 400, and 500 nm
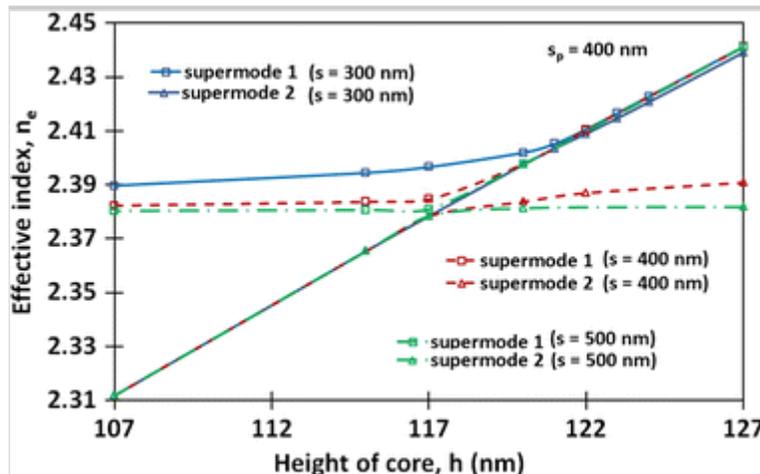
For s = 500 nm the first and second supermodes are shown by dash-dotted green lines with square and triangular symbols, respectively. These two curves appear to intersect at the phase-matching point when h = 117 nm, but in reality the supermodes undergo a transition at this point. When h < 117 nm, the first supermode is the NW mode and the second supermode is the array mode. When h > 117 nm, as the effective index of the array is higher than that of the NW, the first supermode is essentially the array mode. On the other hand, when h < 117 nm, as the effective index of the array is lower than that of the NW, this represents the second supermode. The horizontal line represents the effective index of the NW. At the phase-matching point both the supermodes have equal power in the NW and the array. Similarly, for s = 400 nm the even and odd supermode representing the interaction of the first array mode and NW are plotted here using red dashed line with square and triangular symbols, respectively. It can be observed from this

figure that with reduced spacing, s, the gap between the supermodes at the point of minimum separation between them, increases. Therefore it will be preferable to work at a smaller spacing so that a shorter coupling length can be obtained.

However, for a smaller separation such as s = 300 nm, it was observed that the first two supermodes do not follow the same pattern. As discussed in Sect. 2.1 for $s < s_p$ the NW and array do not behave like the two distinct waveguide sections of the composite structure. Variations of the effective indices of the first and second supermodes of the coupled structure with h for s = 300 nm are also shown in Fig. 9, by solid blue lines with square and triangular symbols, respectively.

In order to keep the coupling length small and obey the design rule of $s > s_p$, the final SSC design has been optimized with s_p = 200 nm and s = 300 nm. Variation of effective indices for the first two supermodes with the thickness h of the SiL for this design has been plotted in Fig. 10. The point of minimum separation between the first two supermodes in this case is h = 89.9 nm. The coupling length for this coupled structure calculated from the difference of the supermodes at h = 89.9 nm is only 288.33 μm.

Fig. 10

Variations of the even and odd supermode effective indices with the core height of the 17-core array, when s_p = 200 nm and s = 300 nm
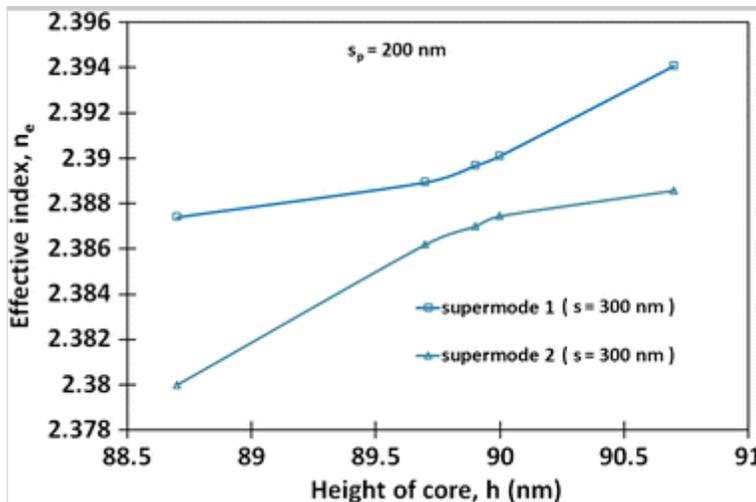

Figure 11a and b show the 1-D field profile of the even and odd supermodes for this coupled structure with h = 89.9 nm, s = 300 nm and s_p = 200 nm, respectively. It can be observed that, the first supermode has an even-like mode profile, but the second supermode has an odd-like field profile with positive and negative fields in the two coupled waveguides. Although the peak field inside the array is smaller,

however, both the guides carry nearly equal power as the array is much larger in both the transverse directions compared to the NW.

Fig. 11

1-D field profile for, **a** supermode 1 and, **b** supermode 2 of the coupled structure for $h = 89.9$ nm, $s_p = 200$ nm and $s = 300$ nm
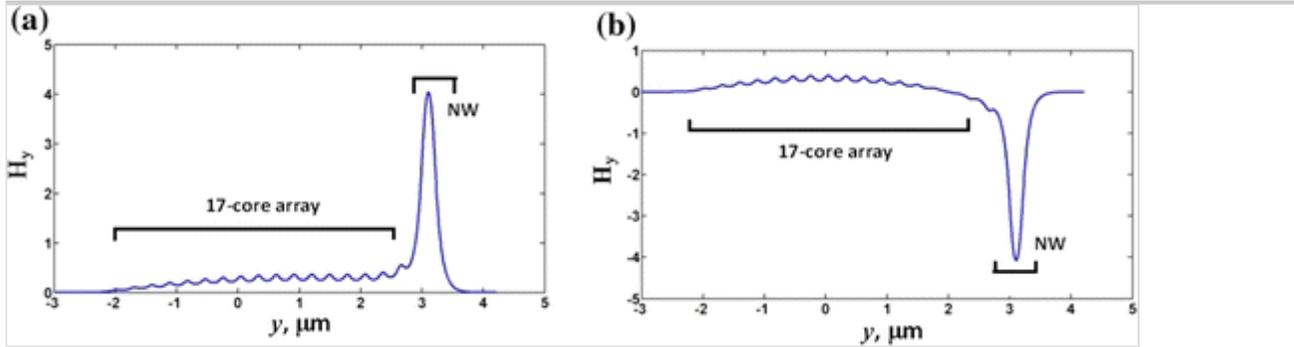
3. Butt-coupling between array and fiber

We used SMF of radius 5 µm having normalized frequency V equal to 2.3 and spot size equal to 87.25 µm². As the expanded spot-size of the SSC was smaller than that of the SMF, it may be useful to find its coupling efficiency to a fiber with smaller radius. Next, we calculated coupling efficiency of the multilayered waveguide array with optical fiber of varying core radius. For these fibers as radius is reduced their index contrast between core and cladding was increased to maintain a constant normalized frequency V equal to 2.3 to satisfy their single-mode operation. Figure 12 shows the transmission coefficients for coupling between a 17-core array with $h = 89.9$ nm and $s_p = 200$ nm and a single-mode fiber with radius varying from 1 to 5 µm. It also shows the transmission coefficients for coupling between the same fiber and the NW for comparison. To evaluate these coefficients we have used the rigorous LSBR method which also takes into account the reflections at the butt-coupled junctions. In case of the array, a transmission coefficient (τ) of 0.57 was observed when coupled to a fiber of radius 5 µm. Therefore, in this case, a power coupling (τ^2) efficiency of 32.5% was obtained compared to only 0.36% $(0.06)^2$ in case of direct coupling of the NW, which suggests a 100 times improvement. The maximum transmission was obtained when the array is coupled to fiber of radius 2 µm, where their A_{eff} values match better and in this case the power coupling was 88.4% ($\tau = 0.94$) as compared to only 2.2% (0.15^2) for the NW. The spot-size for the optimized array is best matched with a high-NA fiber of radius 2 µm, therefore the best transmission is obtained in this case. Figure 13 shows the 2-D modal field plots of the array and the fiber of radius

2 μm which clearly shows the mode-size matching obtained in this case. But as the concept shows, and if needed, the spot-size can be further expanded to couple to a conventional SMF. We have also calculated approximate transmission coefficients using the following analytical equation (Ghatak and Thyagarajan 1991);

Fig. 12

Transmission coefficients from the LSBR and analytical formula for array and nanowire coupling with fiber versus radius of fiber
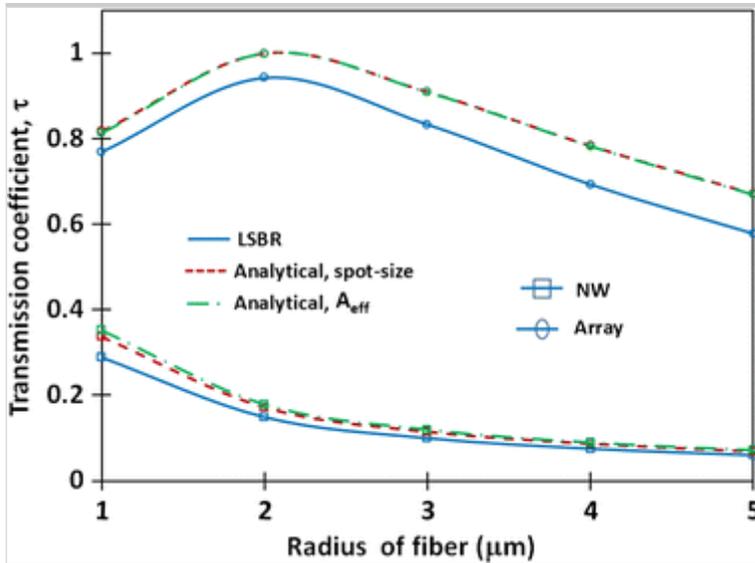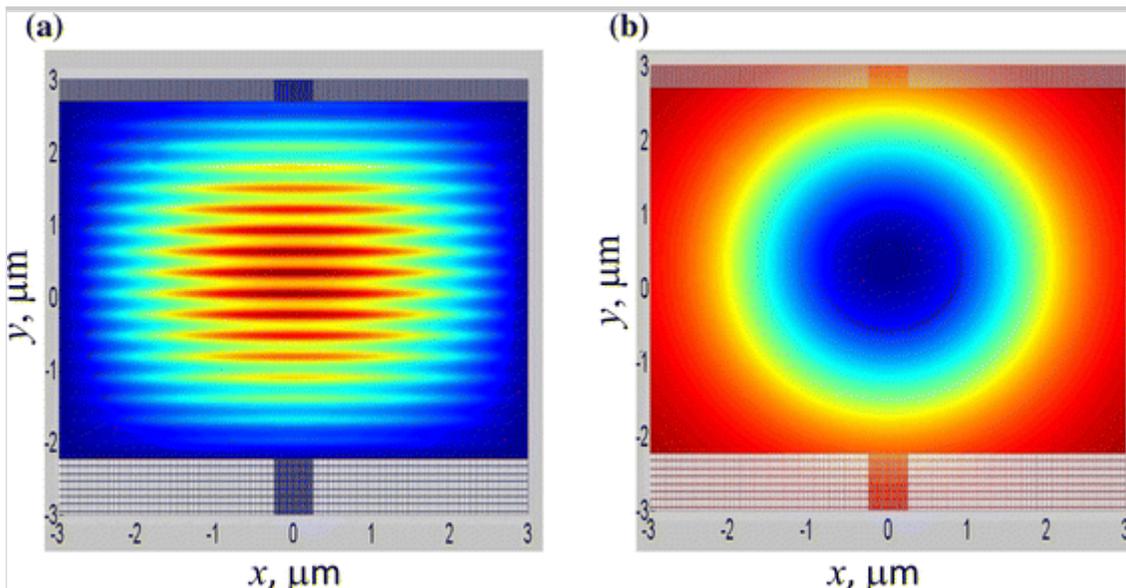

Fig. 13

a 2-D field profile of the array having dimensions $h = 89.9$ nm and $s_p = 200$ nm **b** 2-D field profile of the fiber with radius 2 μm

$$\tau = \frac{2\sigma_1\sigma_2}{\sigma_1^2 + \sigma_2^2} \qquad\qquad 2$$

where, mode-size σ_1 and σ_2 are calculated as the square root of the numerically obtained spot-size or A_{eff} of the fiber and array/NW. Figure 12 shows transmission coefficients, calculated by using approximate Eq. (2) incorporating either the spot-size or the A_{eff}. However, it should be noted that this expression is valid only for Gaussian field profiles. For the array and fiber coupling, it is only an indicative and the LSBR is a rigorous approach, which is used here. The NW field is nearly Gaussian in shape and the fiber field is also Gaussian, therefore the analytical coefficients in this case match well with the LSBR coefficients. It should be noted that the simple analytical equation using the mode area values overestimates the transmission coefficient values.

4. Results and discussion

After finding the supermodes of the coupled structure at the optimized dimensions of $h = 89.9$ nm, $s_p = 200$ nm and s = 300 nm, the LSBR method is used to calculate the power transfer along the length of the SSC. The NW is used to input power into the NW of the SSC at z = 0. We have used only the first and second supermodes for this calculation since the higher order modes of this SSC have negligible excitation coefficients compared to the first 2 supermodes. Moreover, including higher order modes in the LSBR simulations increases the computation time significantly. The excitation coefficients for the first 2 modes are 0.661 and 0.667 respectively. The reflection coefficients for these two modes are 0.062 and 0.61E−4, respectively. Hence, we can conclude that reflections between the NW and SSC at z = 0 are negligible. The coupling length for this SSC at $h = 89.9$ nm is 288.33 μm.

Figure 14 shows the 2-D field profile in this coupled structure at z = 0 μm and z = 288.33 μm. It can be observed from these figures, at z = 0, most of the input power gets butt coupled to the NW of the directional coupler. From the LSBR method we obtain a power transmission of T = 0.882 at z = 0. At z = L = 288.33 μm, most of the butt-coupled power gets evanescently coupled to the fundamental mode of the array as shown in Fig. 14b. However, it was observed that by increasing the number of modes to five, the power transmission goes up to a value of 0.986 at z = 0.

Fig. 14

2-D field profiles in the coupled structure with $h = 89.9$ nm, $s_p = 200$ nm and $s = 300$ nm at **a** $z = 0$ and **b** $z = L = 288.33$ μm
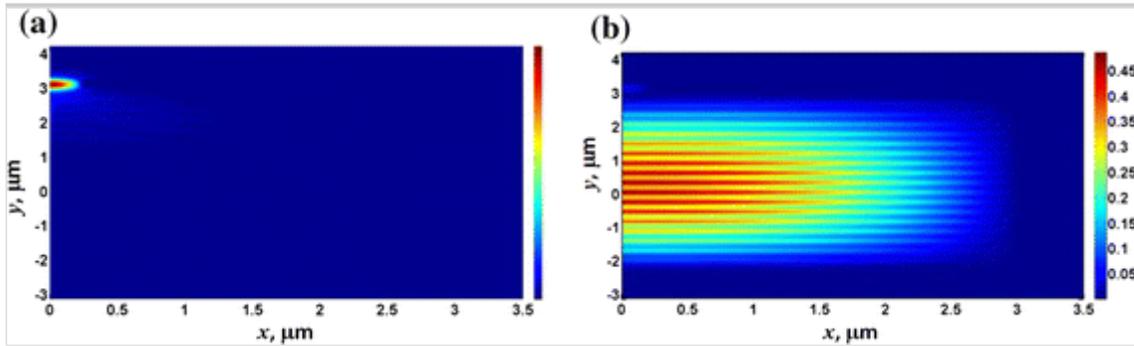

As discussed in Sect. 3, the highest power coupling of the SSC can be obtained with the high-NA fiber of radius 2 μm. Next we calculated the power coupling from the SSC structure at $z = 288.33$ μm to the butt-coupled high-NA fiber of radius 2 μm where a transmission coefficient of value 0.99 was obtained. This is equivalent to power transfer, $T = \tau^2 = 0.98$ (loss of 0.087 dB only) between the SSC and high-NA fiber of radius 2 μm. In simulations we have not assumed an air gap between the SSC and the fiber. In practice, index-matching liquid can be used to reduce reflections. Therefore the overall coupling from the NW to the fiber obtained from these values is approximately 87%, showing only 0.6 dB loss. Also, if we assume negligible contribution from the higher order modes on the output field at $z = 288.33$ μm (which we verified using photon design as discussed in Sect. 2.1), it can be concluded that the efficiency is higher than 87%, for this system.

We have also studied the alignment tolerances between the fiber and the SSC and again used the LSBR method to find power transfer at this interface. Variations of the transmission coefficient, τ, to the fiber with the vertical misalignment in y are shown in Fig. 15, by a solid blue line. Here, zero displacement indicates that the fiber is aligned with the center of the array. Figure 15 shows the maximum transmission coefficient value of 0.99, when the fiber is properly aligned. The field profile at the end of the SSC and that of the fiber are also shown as an inset using a solid blue line and a dashed red line, respectively. It can be observed that their profiles are very similar which yields such a high coupling at this interface. Figure 15 also shows the transmission coefficient variation for a NW directly butt-coupled to the fiber with the displacement in the y direction, by a dashed red line.

Fig. 15

Transmission coefficient versus displacement of fiber in the y-direction for coupling between fiber of radius 2 μm and nanowire/SSC with $h = 89.9$ nm, $s_p = 200$ nm and $s = 300$ nm
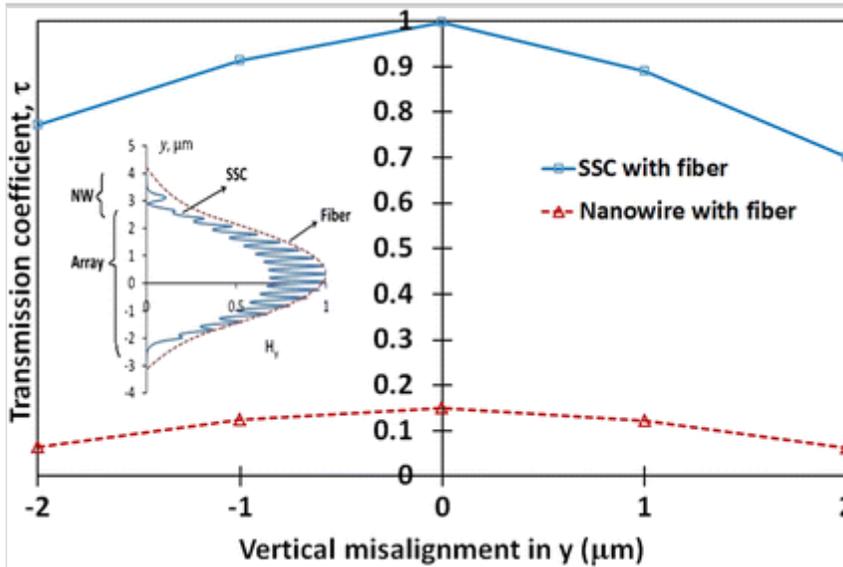
The transmission coefficient drops to 0.77 (59.2%) and 0.7 (49%) with 2 μm displacement in upward and downward directions respectively between the coupled structure and the fiber. It can be observed from Fig. 15 that the 1 dB alignment tolerances are around −1.8 and 1.5 μm in the vertical lower and upper directions, respectively. As shown in Fig. 15, the coupling efficiencies at these tolerances are much higher than in the case of just the NW and the fiber. These tolerances are sufficiently high and comparable to values in recently reported high mode-field diameter tapers (Picard et al. 2016; Sisto et al. 2016). The performance for this improved design will be better than the previous design because the output field will now resemble the first array mode more closely, since the higher order modes of the coupled structure can be neglected in the propagation of power.

As this device was designed for 1.55 μm, the effect of variation of wavelength around 1.55 μm can also be studied but not reported here. However, as we move away from phase-matching the performance will deteriorate. But, if needed a similar design can be achieved for other important telecom wavelengths such as 1.31 μm.

5. Conclusion

We have presented a new improved design version of the recently reported SSC based on the concept of evanescent coupling between a NW and an array made of

parallel Si layers. A new design rule has been proposed in this paper according to which the inner separation of the array has to be kept smaller than the separation between the NW and array. Since the previous structure did not take into consideration this rule, higher order modes of the SSC were also excited at the NW/SSC interface. This can reduce the performance of the SSC. Therefore, based on this rule an optimized spot-size converter with 17-core array having dimensions $h = 89.9$ nm, $s_p = 200$ nm and s $= 300$ nm has been studied. The coupling length for this SSC is calculated to be 288.33 µm at which a high coupling efficiency of 98% (0.087 dB loss only) is recorded. An overall coupling of ~87% is obtained between the NW and high-NA fiber of radius 2 µm showing only 0.6 dB loss whereas direct power coupling from the NW to the SMF of radius 2 µm directly is only 2.2% (16.5 dB loss).

We have also reported relatively high alignment tolerances between this spot-size converter and the SMF which may help in reducing the overall packaging cost of the photonic integrated system. In conclusion, this SSC not only provides high coupling efficiency with a high-NA fiber of radius 2 µm but also sufficiently high alignment tolerances and a small device length. Moreover, it is a taper-free design with CMOS compatible fabrication steps. Therefore this spot-size converter may help achieve a silicon based monolithically integrated optical chip which can be coupled to the single mode fiber in an optical communication system at a lower cost.

Acknowledgements

References

Bakir, B.B., Gyves, A.V.D., Orobtchouk, R., Lyan, P., Porzier, C., Roman, A., Fedeli, J.-M.: Low-Loss (<1 dB) and polarization-insensitive edge fiber couplers fabricated on 200-mm silicon-on-insulator wafers. IEEE Photon Technol. Lett. **22**, 739–741 (2010)

Barh, A., Rahman, B.M.A., Varshney, R.K., Pal, B.P.: Design and performance study of a compact SOI polarization rotator at 1.55 µm. J. Lightwave Technol. **31**, 3687–3693 (2013)

Cheng, Z., Chen, X., Wong, C.Y., Xu, K., Fung, C.K.Y., Chen, Y.M., Tsang, H.K.: Focusing subwavelength grating coupler for mid-infrared suspended membrane waveguide. Opt. Lett. **37**, 1217–1219 (2012a)

Cheng, Z., Chen, X., Wong, C.Y., Xu, K., Tsang, H.K.: Broadband focusing grating couplers for suspended-membrane waveguides. Opt. Lett. **37**, 5181–5183 (2012b)

Cheng, Z., Tsang, H.K.: Experimental demonstration of polarization-insensitive air-cladding grating couplers for silicon-on-insulator waveguides. Opt. Lett. **39**, 2206–2209 (2014)

Fang, Q., Liow, T.Y., Song, J.F., Tan, C.W., Yu, M.B., Lo, G.Q., Kwong, D.L.: Suspended optical fiber-to-waveguide mode size converter for silicon photonics. Opt. Express **18**, 7763–7769 (2010)

Ghatak, A., Thyagarajan, K.: Optical Electronics. Cambridge University Press, Cambridge (1991)

Haxha, S., Ladely, E.O., Mjeku, M., AbdelMalek, F., Rahman, B.M.A.: Optimization of compact lateral, vertical, and combined tapered spot-size converters by use of the beam-propagation method. Appl. Opt. **45**, 288–296 (2006)

Jiang, W., Kohli, N., Sun, X., Rahman, B.M.A.: Multi-poly-silicon-layer based spot-size converter for efficient coupling between silicon waveguide and standard single-mode fiber. IEEE Photon J. **8**, 6600612 (2016)

AQ1

Papes, M., Cheben, P., Benedikovic, D., Schmid, J.H., Pond, J., Halir, R., Moñux, A.O., Pérez, G.W., Ye, W.N., Xu, D.X., Janz, S., Dado, M., Vašinek, V.: Fiber-chip edge coupler with large mode size for silicon photonic wire waveguides. Opt. Express **24**, 5026–5038 (2016)

Picard, M.J., Latrasse, C., Larouche, C., Painchaud, Y., Poulin, M., Pelletier, F., Guy, M.: CMOS-compatible spot-size converter for optical fiber to sub-μm silicon waveguide coupling with low-loss low-wavelength dependence and high tolerance to misalignment. Proc. SPIE. **9752**, 97520W (2016)

Preston, K., Schmidt, B., Lipson, M.: Polysilicon photonic resonators for large-scale 3D integration of optical networks. Opt. Express **15**, 17283–17290 (2007)

Rahman, B.M.A., Davies, J.B.: Finite-element analysis of optical and microwave waveguide problems. IEEE Trans. Microw. Theory Tech. **32**, 20–28 (1984)

Rahman, B. M. A., Davies, J. B.: Vector-H finite element solution of GaAs GaAlAs rib waveguides. IEEE Proc. J. Optoelectron. **132**, 349–353 (1985)

Rahman, B.M.A., Davies, J.B.: Analysis of optical waveguide discontinuities. J. Lightwave Technol. **6**, 52–57 (1988)

Rajarajan, M., Rahman, B.M.A., Wongcharoen, T., Grattan, K.T.V.: Accurate analysis of MMI devices with two-dimensional confinement. J. Lightwave Technol. **14**, 2078–2084 (1996)

Sisto, M.M., Fisette, B., Paultre, J.E., Paquet, A., Desroches, Y.: Novel spot size converter for coupling standard single mode fibers to SOI waveguides. Proc. SPIE. **9752**, 975217 (2016)

Taillaert, D., Bogaerts, W., Bienstman, P., Krauss, T.F., Daele, P.V., Moerman, I., Verstuyft, S., Mesel, K.D., Baets, R.: An out-of-plane grating coupler for efficient butt-coupling between compact planar waveguides and single-mode fibers. IEEE J. Quantum Electron. **38**, 949–955 (2002)

Taillaert, D., Laere, F.V., Ayre, M., Bogaerts, W., Thourhout, D.V., Bienstman, P., Baets, R.: Grating couplers for coupling between optical fibers and nanophotonic waveguides. Jpn. J. Appl. Phys. **45**, 6071–6077 (2006)

Tokushima, M., Kamei, A., Horikawa, T.: Dual-tapered 10-μm-spot-size converter with double core for coupling polarization-independent silicon Rib waveguides to single-mode optical fibers. Appl. Phys. Expr. **5**, 022202 (2012)

Tsuchizawa, T., Yamada, K., Fukuda, H., Watanabe, T., Takahashi, J., Takahashi, M., Shoji, T., Tamechika, E., Itabashi, S., Morita, H.: Microphotonics devices based on silicon microfabrication technology. IEEE J. Sel. Top. Quantum Electron. **11**, 232–240 (2005)

Uthman, M., Rahman, B.M.A., Kejalakshmy, N., Agrawal, A., Abana, H., Grattan, K.T.V.: Stabilized large mode area in tapered photonic crystal fiber for stable coupling. IEEE Photon J. **4**, 340–349 (2012)

Wongcharoen, T., Rahman, B.M.A., Grattan, K.T.V.: Accurate characterization of optical filters with two-dimensional confinement. J. Lightwave Technol. **14**, 2596–2603 (1996)

Wongcharoen, T., Rahman, B.M.A., Rajarajan, M., Grattan, K.T.V.: Spot-size conversion using uniform waveguide sections for efficient laser-fiber coupling. J. Lightwave Technol **19**, 708–716 (2001)